Curcumenol triggered ferroptosis in lung cancer cells via lncRNA H19/miR-19b-3p/FTH1 axis

Ruonan Zhang [a,b,c,d,e], Ting Pan [b,c,d,e], Yu Xiang [b,c,d,e], Mingming Zhang [b,c,d,e], Han Xie [a,b,c,d,e], Zimao Liang [a,b,c,d,e], Bi Chen [a,b,c,d,e], Cong Xu [a], Jing Wang [a], Xingxing Huang [a,b,c,d,e], Qianru Zhu [a,b,c,d,e], Ziming Zhao [a], Quan Gao [b,c,d,e], Chengyong Wen [b,c,d,e], Wencheng Liu [b,c,d,e], Weirui Ma [b,c,d,e], Jiao Feng [b,c,d,e], Xueni Sun [b,c,d,e], Ting Duan [b,c,d,e], Elaine Lai-Han Leung [a], Tian Xie [b,c,d,e,*], Qibiao Wu [a,f,**], Xinbing Sui [a,b,c,d,e,***]

[a] State Key Laboratory of Quality Research in Chinese Medicines, Faculty of Chinese Medicine, Macau University of Science and Technology, Macau
[b] School of Pharmacy and Department of Medical Oncology, The Affiliated Hospital of Hangzhou Normal University, School of Medicine, Hangzhou Normal University, Hangzhou, 311121, Zhejiang, China
[c] Key Laboratory of Elemene Class Anti-Cancer Chinese Medicines, China
[d] Engineering Laboratory of Development and Application of Traditional Chinese Medicines, China
[e] Collaborative Innovation Center of Traditional Chinese Medicines of Zhejiang Province, Hangzhou Normal University, Hangzhou, 311121, Zhejiang, China
[f] Guangdong-Hong Kong-Macao Joint Laboratory for Contaminants Exposure and Health, Guangzhou, 510006, China

ARTICLE INFO

ABSTRACT

Curcumenol, an effective ingredient of Wenyujin, has been reported that exerted its antitumor potential in a few cancer types. However, the effect and molecular mechanism of curcumenol in lung cancer are largely unknown. Here, we found that curcumenol induced cell death and suppressed cell proliferation in lung cancer cells. Next, we demonstrated that ferroptosis was the predominant method that contributed to curcumenol-induced cell death of lung cancer *in vitro* and *vivo* for the first time. Subsequently, using RNA sequencing, we found that the long non-coding RNA H19 (lncRNA H19) was significantly downregulated in lung cancer cells treated with curcumenol, when compared to untreated controls. Overexpression of lncRNA H19 eliminated the anticancer effect of curcumenol, while lncRNA H19 knockdown promoted ferroptosis induced by curcumenol treatment. Mechanistically, we showed that lncRNA H19 functioned as a competing endogenous RNA to bind to miR-19b-3p, thereby enhanced the transcription activity of its endogenous target, ferritin heavy chain 1 (FTH1), a marker of ferroptosis. In conclusion, our data show that the natural product curcumenol exerted its antitumor effects on lung cancer by triggering ferroptosis, and the lncRNA H19/miR-19b-3p/FTH1 axis plays an essential role in curcumenol-induced ferroptotic cell death. Therefore, our findings will hopefully provide a valuable drug for treating lung cancer patients.

1. Introduction

Among the most common cancer types, lung cancer is the major cause of cancer-related deaths worldwide [1]. Currently available treatment strategies for lung cancer patients include surgery, chemotherapy, radiotherapy, molecular target therapy, immunity therapy, and photodynamic or laser therapy [2]. Although many improvements in the management of advanced lung cancer have been made, the therapeutic

efficacy of these agents is limited due to their associated severe adverse effects, dose-limiting toxicity, drug resistance, and poor selectivity [3]. Thus, developing new therapeutic strategies or new effective drugs for lung cancer treatment is urgently required.

The development of traditional Chinese medicine is driven by its low toxicity and high efficiency [4]. Curcumenol, a natural product isolated from Curcuma wenyujin, has been reported to have antitumor potential in a few cancer types. Curcumenol showed a cytotoxic effect on human gastric cancer AGS cells by inducing cell apoptosis [5,6]. Curcumenol inhibited the proliferation and metastasis of liver cancer via reducing endogenous H_2S levels [7]. Curcumenol could also suppress the growth and invasion of breast cancer [8,9]. Nevertheless, the effect and molecular mechanism of curcumenol in lung cancer are largely unknown.

As a new pattern of iron-dependent cell death, ferroptosis is distinct from other cell death types, for instance, autophagy, apoptosis, necrosis, and pyroptosis. This cell death form is featured with iron (Fe^{2+})-dependent lipid peroxidation, depletion of the endogenous antioxidant glutathione (GSH), and altered mitochondrial morphology [10,11]. In recent years, stimulating ferroptosis has become a potential strategy that eliminates cancer cells, especially for drug-resistant malignancies. As a critical source of developing novel anticancer compounds, many active ingredients of traditional Chinese medicine are proved to regulate ferroptosis in cancer cells [12]. However, there is no related report about the relationship between curcumenol and ferroptosis.

Non-coding RNAs (ncRNAs), especially long non-coding RNAs (lncRNAs) and microRNAs (miRNAs) have been involved in diverse biological processes, including apoptosis, autophagy, cell cycle arrest, differentiation, immune response, and tumor initiation [13,14]. Furthermore, the function of lncRNAs as competing for endogenous RNAs (ceRNAs) has attracted increasing attention as a "miRNA sponge" to destroy miRNA-mediated degradation of target mRNAs [15]. For example, lncRNA LCAT1 functioned as a ceRNA to up-regulate the activity of RAC1 by sponging miR-4715-5p to promote the progression of lung cancer [16]. LncRNA PVT1 sponged the miR-619-5p and increased the expression of Pygo2 and ATG14, which promoted gemcitabine resistance in pancreatic cancer by up-regulation of Wnt/β-catenin and autophagy pathway [17]. LncRNA H19-derived miR-let-7 contributed to glucose metabolism in muscle cells [18]. Therefore, lncRNAs or derived miRNAs play a crucial role in tumorigenesis and cancer development. However, the role and molecular mechanisms of lncRNAs in the anticancer effect of natural products require further investigation.

In our studies, we investigated the impact of curcumenol on lung cancer cells H1299 and H460. The results revealed that curcumenol exhibited its anticancer activity by triggering ferroptosis both *in vitro* and *in vivo*. Subsequently, we showed that the lncRNA H19/miR-19b-3p/FTH1 axis (Scheme 1) was a key determinant for curcumenol-induced ferroptotic cell death of lung cancer. Our findings will hopefully provide a valuable natural product for lung cancer treatment.

2. Materials and methods

2.1. Cell culture

Human lung fibroblast cells (CCD19), human normal lung epithelial
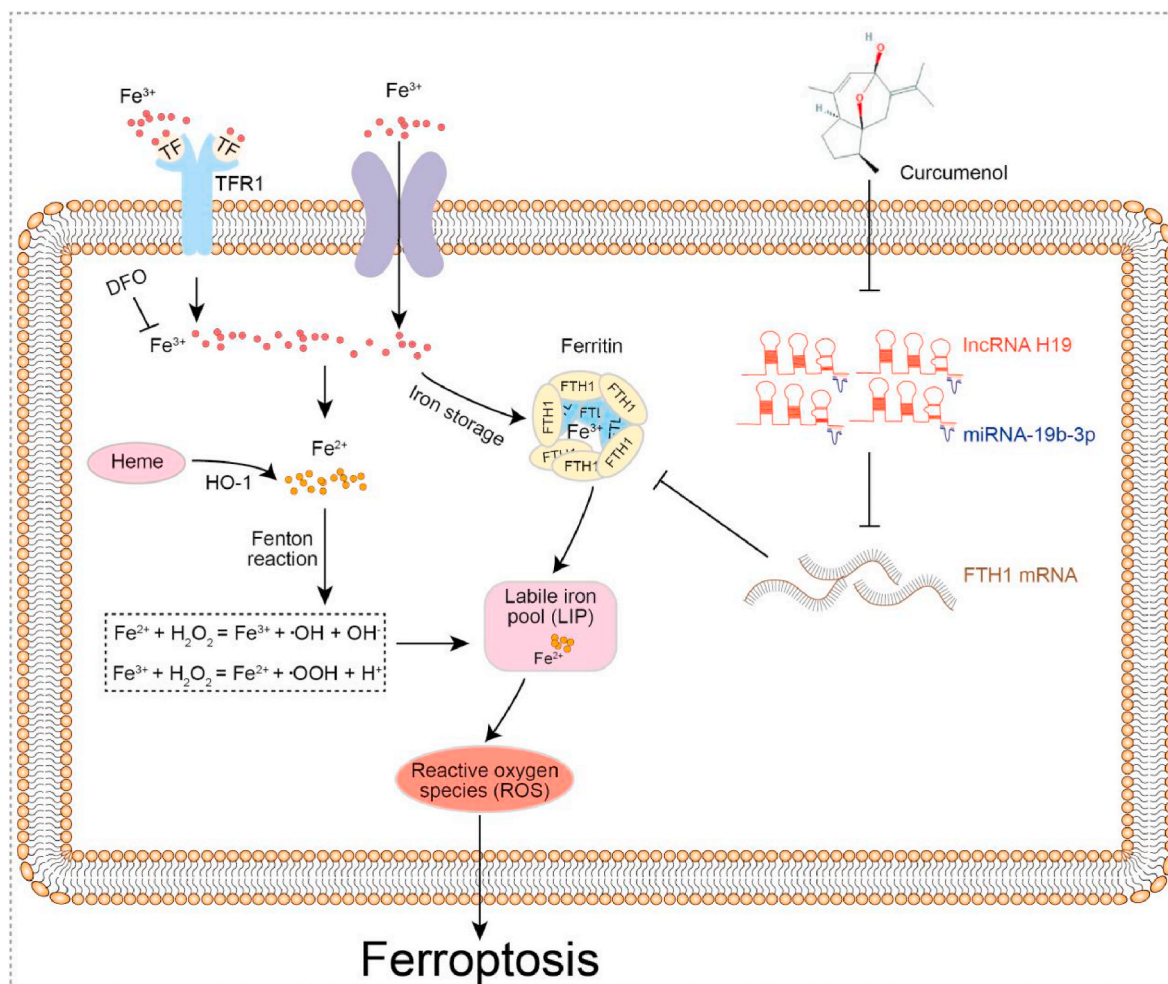
Scheme 1. Schematic illustration of curcumenol-induced ferroptosis via lncRNA H19/miR-19b-3p/FTH1 axis in lung cancer cells.

cells (BEAS-2B), human lung cancer cells (H1299 and H460), and human embryonic kidney cells (293T) were bought from American Type Culture Collection (ATCC). CCD19, H1299 and H460 cells were cultured in RPMI-1640 medium containing 10% fetal bovine serum (FBS) and 1% Penicillin-Streptomycin (PS). BEAS-2B cells were grown in a BEGM medium. HEK293T cells were cultured with Dulbecco's Modified Eagle Medium (DMEM) medium supplemented with 10% FBS and 1% PS. All cells were maintained at 37 °C, 5% CO_2 incubator.

2.2. Reagents and antibodies

Purified curcumenol (>98%) (A1069) was bought from CHENGDU MUST BIO-TECHNOLOGY CO., LTD. A stock solution of curcumenol was prepared in methanol (Sigma-Aldrich, 34860) at 100 mg/ml. Deferoxamine (HY–B0988), Ferrostatin-1 (HY-100579), necrostatin-1 (HY-15760), Z-VAD-FMK (HY–16658B), chloroquine (HY-17589A), and Liproxstatin-1 (HY-12726) were purchased from MCE.

The antibodies used were anti-GAPDH (Cell Signaling, 5174), anti-GPX4 (abcam, ab125066), anti-FTH1 (abcam, ab65080), anti-Transferrin (abcam, ab82411), anti-SLC7A11 (abcam, ab37185), anti-Heme Oxygenase-1 (HO-1) (abcam, ab13248), anti-SLC40A1 (abcam, ab239583), anti-NRF2 (Cell Signaling, 12721), anti-rabbit IgG (H+L), Biotinylated Antibody (Cell Signaling, 14708), Anti-mouse IgG (H+L), Biotinylated Antibody (Cell Signaling, 14709). All antibodies were used at 1:1000 dilution.

Lentiviral vectors pCAG-dR8.9 (D8216) and pCMV-VSV-G (D8215) were purchased from Beyotime. TAT Human Tagged ORF Clone (RC216782) and REV Virus Tagged ORF Clone (VC101717) were purchased from Origene. Both negative control (NC), lncRNA H19, lv3-shNC plasmids, lv3-shH19 plasmids, miR-19b-3p mimic, miR-19b-3p inhibitor and inhibitor NC were designed by GenePharma. Lipofectamine™ 3000 Transfection Reagent (L3000015) was purchased from Thermo Fisher Scientific.

2.3. Cytotoxicity and apoptosis

The cytotoxicity of curcumenol in lung cancer cells was determined with Cell Counting Kit-8 (CCK-8) (LJ621, Dojindo, Japan). Cell apoptosis was measured by Flow cytometry using Phartmingen Annexin V–FITC Apoptosis Detection Kit I (556547, BD, USA).

2.4. Colony-formation assay

H1299 and H460 cells were plated in 6-well plates and replaced the medium every 2–3 days. Add the medium with or without curcumenol until the cell colonies can be observed under a microscope. At the end of the experiment, cells were fixed and stained using the Crystal Violet Solution 2.5% in methanol (G1064, Solarbio). Colonies were manually scored blindly and quantified by ImageJ.

2.5. qRT-PCR

Total RNA was prepared by TRIzol (Invitrogen, CA, USA) and reverse transcribed to cDNA by TransScript All-in-One First-Strand cDNA Synthesis SuperMix for qPCR (One-Step gDNA Removal) (TransGen Biotech, AT341-03). PerfectStart Green qPCR SuperMix (+Dye II) (TransGen Biotech, AQ602-23) was used to analyze the mRNA expression. 1 μg total RNA was reverse transcribed using the miRNA 1st Strand cDNA Synthesis Kit (by stem-loop) (Vazyme, MR101). miRNA Universal SYBR qPCR Master Mix (Vazyme, MQ101) was used to analyze the miRNA expression. The sequences of all qPCR primers used in our research are listed in Table 1. The $2^{-\Delta\Delta Ct}$ method was used to analyze the qRT-PCR results. The sequence of miR-19b-3p mimics and miR-19b-3p inhibitor are as follows [20]:

miR-19b-3p mimics:
5′-UGUGCAAAUCCAUGCAAAACUGA-3'

Table 1
Primers sequence for Real-Time qPCR.

Gene	Forward primer	Reverse primer
GAPDH	AGCCACATCGCTCAGACAC	GCCCAATACGACCAAATCC
FTH1	TGAAGCTGCAGAACCAACGAGG	GCACACTCCATTGCATTCAGCC
GPX4	ACAAGAACGGCTGCGTGGTGAA	GCCACACACTTGTGGAGCTAGA
Transferrin	TCAGCAGAGACCACCGAAGACT	GACCACACTTGCCCGCTATGTA
SLC7A11	TCCTGCTTTGGCTCCATGAACG	AGAGGAGTGTGCTTGCGGACAT
HO-1	CCAGGCAGAGAATGCTGAGTTC	AAGACTGGGCTCTCCTTGTTGC
NRF2	GCTCAAACTTAGGGGCTCCG	GAAGTTGCGGGAAGGTCTGG
lncRNA H19	TCCCAGAACCCACAACATGAA	TTCACCTTCCAGAGCCGATTC
U6	CTCGCTTCGGCAGCACA	AACGCTTCACGAATTTGCGT
miR-19b-3p	CGTGTGCAAATCCATGCAA	CGTGTGCAAATCCATGCAA
miR-181a-5p	CGAACATTCAACGCTGTCG	CGTGTGCAAATCCATGCAA
miR-200b	GATGACGGCGGAGCCC	CGTGTGCAAATCCATGCAA
miR-675	GCCCTCACCGCTCAGCC	CGTGTGCAAATCCATGCAA

3′-AGUUUUGCAUGGAUUUGCACAUU-5'
miR-19b-3p inhibitor:
5′-UCAGUUUUGCAUGGAUUUGCACA-3'

2.6. Measurement of intracellular chelate iron

Intracellular chelate iron levels were measured using Phen Green SK (green) (Thermo Fisher scientific, P14313). Briefly, H1299 and H460 cells were treated with or without curcumenol for 24 h, then incubated with 1 μM Phen Green SK (green) at 37 °C for 15 min. Finally, the cells were observed and taken pictures under a confocal microscope.

2.7. Measurement of ROS

Intracellular ROS levels were measured by the DCFH-DA oxidative stress indicator (Beyotime, S0033) following the recommended manuals. Briefly, H1299 and H460 cells were incubated with serum-free medium containing DCFH-DA at 37 °C for 30 min. Finally, the cells were harvested, and fluorescence signals were determined by flow cytometry.

2.8. Malondialdehyde (MDA) assay

Intracellular lipid peroxidation product malondialdehyde (MDA) was quantified as an indicator of lipid peroxidation. The MDA levels were detected using Lipid Peroxidation MDA Assay Kit (Beyotime, S0131).

2.9. GSH assay

The level of GSH was measured by GSH Assay Kit (Nanjing Jiancheng Bioengineering Institute, A006-2-1) and GSH concentration was calculated according to the instructions.

2.10. Western blotting

Cells were harvested and lysis with RIPA buffer (Beyotime, P0013B), which contained 1 mM PMSF (Beyotime, ST506). The protein concentrations were measured by BCA Protein Assay Kit (Beyotime, P0012S), and the appropriate amount of protein sample was loaded on SDS-polyacrylamide gels. After electrophoresis, samples were transferred to a PVDF membrane. Blocking, incubation with primary and secondary antibodies, and then developed with enhanced chemiluminescence.

2.11. Cell transfection and construction of stably transfected cell lines

H1299 and H460 cells were transfected using Lipofectamine™ 3000

Transfection Reagent (Thermo Fisher Scientific, L3000015) according to the manufacturer's protocol. 293T cells were co-transfected with lv3-shH19, GAG, TAT, VSV, and REV plasmids for lentivirus production. Virus supernatants were collected at 72 h post-transfection. H1299 and H460 cells were infected with virus solution, the medium was changed after 24 h, and the cells were cultured for another 48 h. The cells were either used for the experiment or selected with puromycin (2 μg/ml) for further analysis.

2.12. RNA sequencing

Total RNA was prepared by TRIzol (Invitrogen, CA, USA). Illumina HiSeq 4000 sequencing was performed by LC-BIO Technologies (Hangzhou) Co., LTD. The OmicStudio tools at https://www.omicstudio.cn/tool were used for bioinformatic analysis.

2.13. Tumor xenograft model in vivo

All animal experiments were agreed with the Use and Care of Animals Committee at Hangzhou Normal University. A subcutaneous tumor-bearing nude mouse model was established by injecting the flank of BALB/c nude mice with 5×10^6 H460 cells. Ten days later, mice were blindly randomized into four groups and intravenously injected with 200 μl ddH$_2$O containing 0.1% CMC-Na and 1% Tween 80, iron chelators DFO (100 mg/kg/day), curcumenol (200 mg/kg/day), and curcumenol combine DFO. Tumor long diameter, short diameter, and body weight were detected every two days after the first drug treatment. The tumor volume calculation formula: (tumor long diameter × tumor short diameter^2)/2. Finally, mice were sacrificed. All tumors were collected for immunohistochemical (IHC) staining.

2.14. Statistical analysis

Statistical analyses and graphing were done using GraphPad Prism 9.0 software. Data in our study were represented as mean ± SD. $p < 0.05$ was regarded as statistically significant.

3. Results

3.1. Curcumenol induced cell death and suppressed cell proliferation in lung cancer cells

To evaluate the anticancer potential of curcumenol on lung cancer, different concentrations of curcumenol were treated in the human lung fibroblast cells (CCD19), human normal lung epithelial cells (BEAS-2B) and lung cancer cells (H1299 and H460) for 24 h. We found that curcumenol had the potential to suppress cell survival in a concentration-dependent manner in lung cancer cells, but with relatively minor toxicity in normal lung cells (Fig. 1A and B), indicating that curcumenol was selectively cytotoxic to lung cancer cells. Next, the clonogenic assay was used to detect the effect of curcumenol on cell proliferation. As shown in Fig. 1C and D, compared with control, curcumenol dramatically inhibited the colony formation of lung cancer cells in a dose-dependent manner. To evaluate the effect of curcumenol on the cell death of H1299 and H460 cells, the Annexin V-FITC/PI staining was analyzed by flow cytometry. As expected, compared with control, a high percentage of the dead cells was observed in lung cancer cells after with curcumenol treatment. Nevertheless, overall apoptosis was lower (Fig. 1E and F), perhaps due to apoptosis not be the predominant pattern of cell death induced by curcumenol. In summary, these data suggested that curcumenol reduced cell viability and induced cell death in lung cancer cells.

3.2. Ferroptosis as the predominate method contributed to curcumenol-induced cell death in lung cancer cells

In order to evaluate the main cell death program induced by curcumenol, we used specific inhibitors, including necrostatin-1 (Nec-1, necroptosis inhibitor), chloroquine (CQ, autophagy inhibitor), Z-VAD (pan-caspase inhibitor), and the ferroptosis inhibitor deferoxamine (DFO), Ferrostatin (Fer-1) and liproxstatin-1 (Lip-1). The results showed that Nec-1, Z-VAD and CQ could not remarkably inhibit the cell death caused by curcumenol in H1299 and H460 cells (Fig. 2A–C). However, the ferroptosis inhibitor DFO, Fer-1 and Lip-1 significantly rescued curcumenol-induced cell death (Fig. 2D–F). These results proved that ferroptosis might be a predominant cell death program for curcumenol-induced cell death.

To further determine whether curcumenol-induced cell death through ferroptosis, ferroptosis-related proteins were examined by western blotting. Our data showed that curcumenol treatment remarkably increased the expression levels of heme oxygenase 1 (HO-1) and transferrin but decreased the expression levels of glutathione peroxidase 4 (GPX4), solute carrier family 40 member 1 (SLC40A1), solute carrier family 7 member 11 (SLC7A11), ferritin heavy chain 1 (FTH1), Nuclear factor E2-related factor 2 (NRF2) and glutaminase in lung cancer cells (Fig. 3A). Moreover, iron chelator DFO could rescue the expression of ferroptotic proteins induced by curcumenol treatment (Fig. 3B).

In the subsequent experiments, RNA-sequencing was performed to investigate the differential transcriptomic response to curcumenol treatment. Differential expression genes were screened and identified by digital gene expression profiling. The differential expression genes were classified into Gene Ontology (GO) categories and Kyoto Encyclopedia of Genes and Genomes (KEGG) pathways in further study. As a result, 1665 upregulated and 1232 downregulated genes were identified in H1299 cells (Fig. S1A). 1484 upregulated and 759 downregulated genes were identified in H460 cells (Fig. S1B). The GO enrichment analyses showed that the oxidation-reduction process and oxidoreductase activity were enriched (Figs. S1C and D). Meanwhile, KEGG analyses discovered that ferroptosis pathways were enriched (Fig. 3C and D). These results suggested that lung cancer cells undergo ferroptosis upon the treatment with curcumenol.

As we all know, reactive oxygen species (ROS) accumulation, GSH depletion, lipid peroxidation and redox-active iron overload were critical events in the ferroptosis process [19]. Thus, the levels of intracellular ROS, GSH, the oxidative stress marker malondialdehyde (MDA) and intracellular chelate iron were detected. As expected, the increased ROS level (Fig. 4A) and the decreased GSH level (Fig. 4B and C) were observed following curcumenol treatment. Moreover, the iron chelator DFO could eliminate GSH depletion induced by curcumenol (Fig. 4D and E). Meanwhile, curcumenol treatment upregulated the MDA level in lung cancer cells (Fig. 4F). Additionally, iron-sensitive fluorophore Phen Green SK was used to monitor the intracellular chelate iron, which was quenched upon binding to iron. As anticipated, compared with a control group, the curcumenol treatment decreased the ratio of Phen Green SK-positive cells, and iron chelator DFO could eliminate this phenomenon (Fig. 4G), indicating that ferroptosis was triggered. So, these results suggested that ferroptosis was the primary mechanism by which curcumenol triggered cell death in lung cancer cells.

3.3. Curcumenol triggered ferropotosis in lung cancer xenograft model

To evaluate the antitumor efficacy of curcumenol *in vivo*, the lung cancer subcutaneous xenograft model was established. After the tumor volume reached 80–100 mm^3, the mice with subcutaneous xenografts were randomized to treatment with solvent, curcumenol (200 mg/kg/d), DFO (100 mg/kg/d), and drug combination. Our data showed that curcumenol dramatically inhibited the growth of xenograft tumors and the antitumor effect of curcumenol could be abolished by ferroptosis inhibitor DFO (Fig. 5A and B). However, there was no statistical
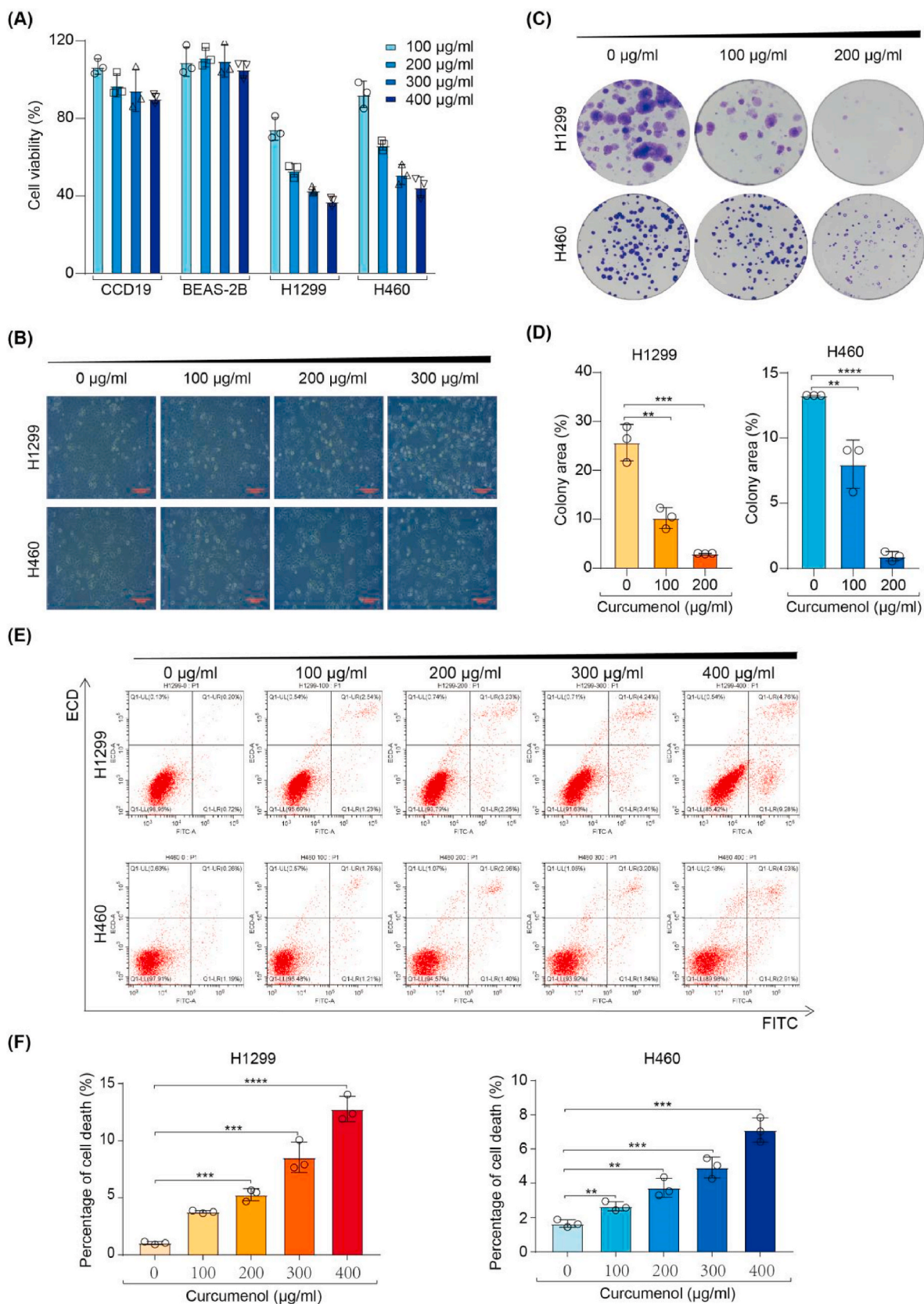
Fig. 1. The cell viability of H1299 and H460 cells was detected after curcumenol treatment. (A) CCD19, BEAS-2B, H1299 and H460 cells were treated with different concentrations of curcumenol for 24 h, and cell viability was measured by CCK8 assay. (B) The cells morphology change was detected under a microscope after the treatment with curcumenol for 24 h. (C, D) Representative results of the colony formation and quantitative analysis. (E, F) Representative results of annexin V-FITC/ PI staining and quantitative analysis after the treatment with curcumenol for 24 h. The mean ± s.d. is shown. **$P < 0.01$, ***$P < 0.001$, ****$P < 0.0001$, n = 3.
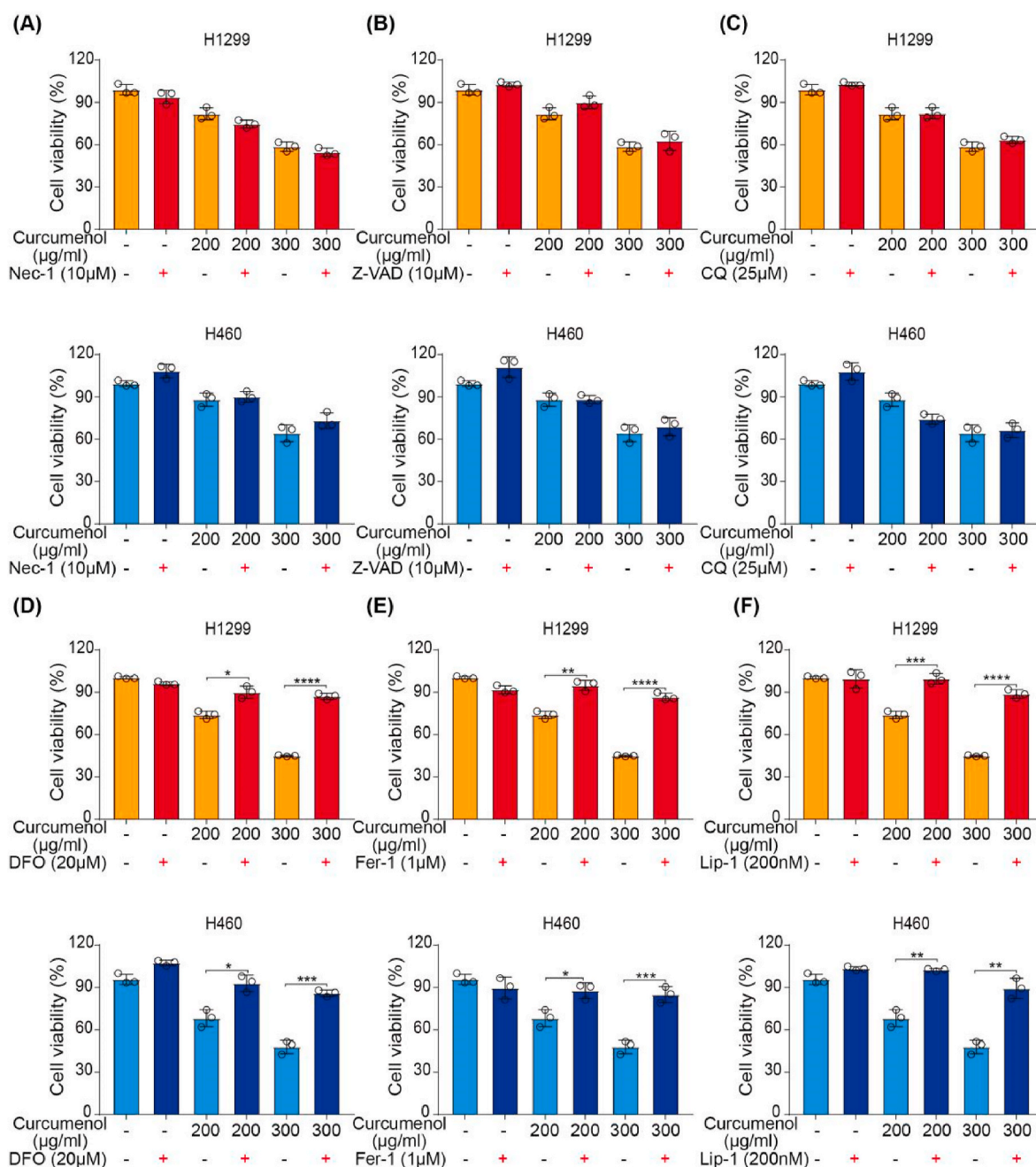
Fig. 2. The effect of curcumenol alone or combines with different cell death inhibitors on the cell viability of lung cancer cells. (A) H1299 and H460 cells were treated with curcumenol with or without Nec-1 (10 μM) for 24 h, and cell viability was detected. (B) H1299 and H460 cells were treated with curcumenol with or without Z-VAD (10 μM) for 24 h, the cell viability was detected. (C) H1299 and H460 cells were treated with curcumenol with or without CQ (25 μM) for 24 h, the cell viability was detected. (D) H1299 and H460 cells were treated with curcumenol with or without DFO (20 μM) for 24 h, and the cell viability was analyzed. (E) H1299 and H460 cells were treated with curcumenol with or without Fer-1 (1 μM) for 24 h, and the cell viability was analyzed. (F) H1299 and H460 cells were treated with curcumenol with or without Lip-1 (200 nM) for 24 h, the cell viability was detected. *$P < 0.05$, **$P < 0.01$, ***$P < 0.001$, ****$P < 0.0001$, n = 3.

difference in body weight between the control and curcumenol treatment group (Fig. 5C), suggesting no apparent toxicity of curcumenol. In further research, we studied the effects of curcumenol on ferroptosis through immunohistochemical (IHC). The decreased levels of GPX4, FTH1 and SLC7A11 and increased expressions of HO-1 and transferrin were found following the curcumenol treatment, indicating curcumenol triggered ferroptosis. Furthermore, the cell death induced by curcumenol was almost eliminated by co-treatment with iron chelator DFO (Fig. 5D). In summary, our results suggested that curcumenol induced ferroptosis in lung cancer *in vivo*.

3.4. The correlation between lncRNA H19 expression and curcumenol-induced ferroptosis

To identify the role of lncRNAs in the anticancer effect of curcumenol, RNA sequencing was performed. We showed that lncRNA H19 was remarkably down-regulated in lung cancer cells treated with curcumenol than untreated ones (Fig. 6A). A similar result was further confirmed by qRT-PCR (Fig. 6B). To investigate the biological function of lncRNA H19 on curcumenol-induced ferroptosis, we overexpressed or knocked down lncRNA H19 in H1299 and H460 cells by transfecting them with an overexpression plasmid or with shRNA, respectively. lncRNA H19
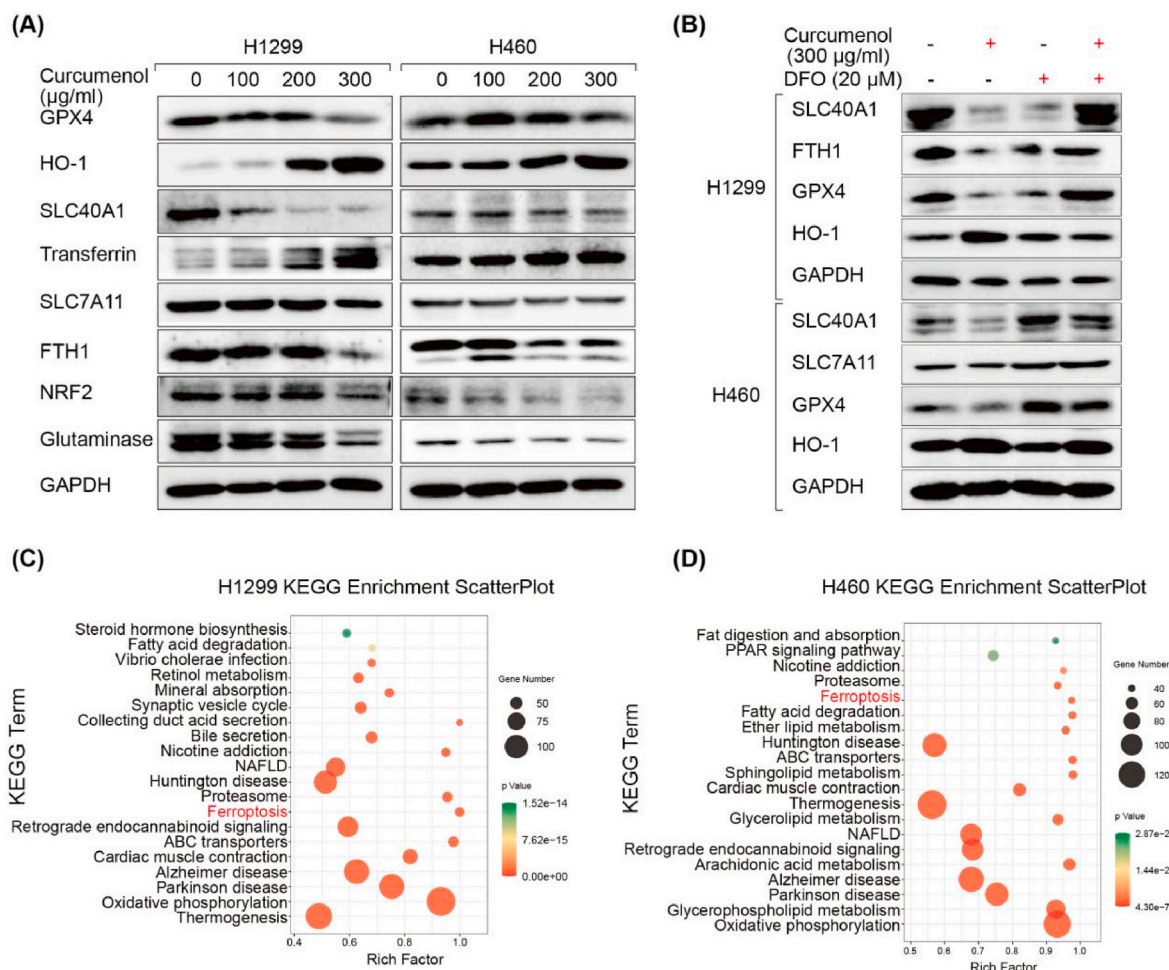
Fig. 3. Ferroptosis was triggered by curcumenol in lung cancer cells. (A–B) The expression of ferroptosis-related proteins in lung cancer cells was detected after curcumenol treatment with or without DFO (20 μM) for 24 h by western blotting. (C, D) KEGG pathway enrichment analysis was performed in H1299 and H460 cells.

overexpression significantly increased the expression levels of ferroptosis negative regulatory factors (NRF2, GPX4, FTH1, and SLC7A11) (Fig. 6C–E). In contrast, lncRNA H19 knockdown significantly decreased the expression levels of ferroptosis negative regulatory factors (NRF2, GPX4, FTH1, and SLC7A11) (Fig. 6F–H). Therefore, our results suggest lncRNA H19 was involved in the ferroptosis induced by curcumenol treatment.

To examine the effects of lncRNA H19 on curcumenol-induced ferroptosis, H1299 and H460 cells were transfected with an overexpression plasmid or with shRNA. The colony formation assay and CCK-8 results showed that lncRNA H19 overexpression significantly abrogated the inhibiting effects of curcumenol in H1299 and H460 cells (Fig. 7A–F). On the contrary, lncRNA H19 knockdown remarkably inhibited the clone formation of H1299 and H460 cells and enhanced the anticancer effect of curcumenol on these cells (Fig. 7G-L). In summary, these data indicate lncRNA H19 was a key determinant for curcumenol-induced ferroptosis.
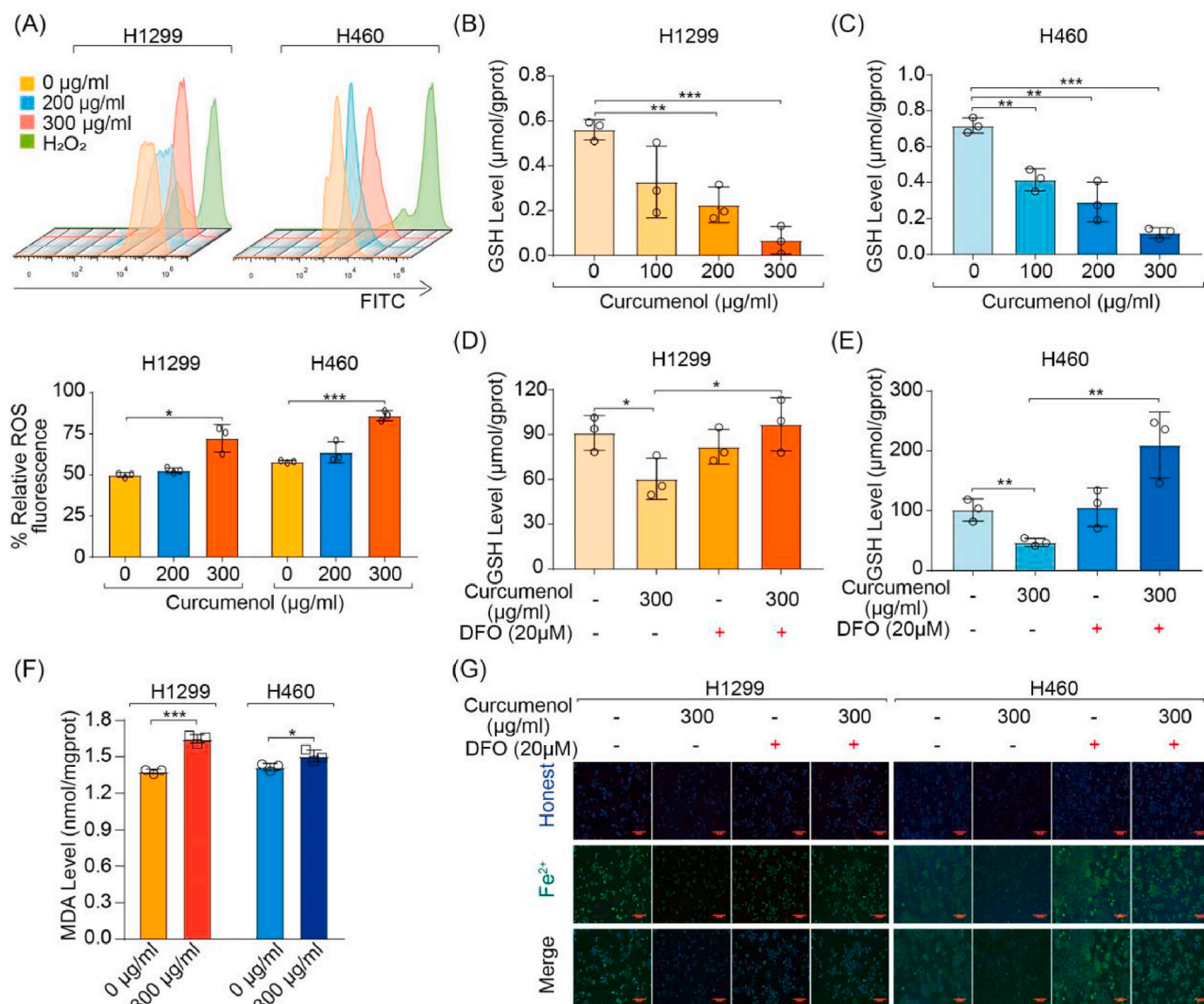
3.5. Curcumenol induced ferroptosis in lung cancer cells via lncRNA H19/miR-19b-3p/FTH1 axis

Growing evidence has demonstrated that lncRNAs can regulate target gene expression through acting as a ceRNA or interacting with RNA-binding proteins. So, we constructed ceRNA networks based on lncRNA-miRNA and miRNA-mRNA interactions used by the bioinformatics database (Starbase) and published literature [20], then founded that lncRNA H19 might target miR-181a-5p, miR-19b-3p, miR-200b and

miR-675 (Fig. S2A). Among the four candidate miRNAs, compared with control, the expression levels of miRNA-19b-3p in H1299 and H460 cells were significantly increased after curcumenol treatment (Fig. 8A–C). Interestingly, a negative correlation was found between miR-19b-3p and FTH1 in lung squamous cell carcinoma (Fig. 8D) and adenocarcinoma (Fig. S2B) in Pan-cancer analysis. Since we have demonstrated that lncRNA H19 could regulate FTH1 expression in H1299 and H460 cells (Fig. 6C–H), it was reasonable to speculate that lncRNA H19 regulated FTH1 levels by targeting miR-19b-3p. The results showed that lncRNA H19 overexpression inhibited the miR-19b-3p level in H1299 and H460 cells (Fig. 8E). In contrast, lncRNA H19 knockdown enhanced the expression of miR-19b-3p in H1299 and H460 cells (Fig. 8F). Meanwhile, we found that miR-19b-3p mimics deceased the FTH1 expression, but increased the anticancer activity of curcumenol in H1299 and H460 cells (Fig. 8G-L). On the contrary, miR-19b-3p inhibitor increased FTH1 expression but abrogated the anticancer activity of curcumenol in H1299 and H460 cells (Fig. 8M–R). These data showed that curcumenol triggered ferroptosis in lung cancer cells via lncRNA H19/miR-19b-3p/FTH1 axis.

4. Discussion and conclusions

Lung cancer is one of the primary causes of cancer deaths globally. Although multiple therapeutic methods are being constructed to combat lung cancer, many challenges remain, especially significant limitations in antitumor effect [21]. Therefore, it urgently needs to develop new agents for lung cancer patients. Natural products with anticancer

Fig. 4. Ferroptosis contributed to curcumenol-induced cell death in lung cancer cells. (A) H1299 and H460 cells were treated with curcumenol for 24 h. 100 μM H₂O₂ was used as a positive indicator, and ROS levels were analyzed by flow cytometer. (B, C) H1299 and H460 cells were treated with curcumenol for 24 h, then GSH levels were detected. (D, E) H1299 and H460 cells were treated with curcumenol with or without DFO (20 μM) for 24 h, and the GSH levels were analyzed. (F) The MDA levels were assayed after the treatment with curcumenol (300 μg/ml) for 24 h. (G) H1299 and H460 cells were treated with curcumenol with or without DFO (20 μM) for 24 h, and intracellular chelate iron was analyzed. *P < 0.05, **P < 0.01, ***P < 0.001, n = 3.

activity have received increasing attention in the past few years due to their excellent safety and efficacy profiles. Paclitaxel, a natural product isolated from the bark of Taxus brevifolia, in combination with lapatinib in nanocolloids, overcame the multidrug-resistant in the ovarian cancer cell line [22]. The stable co-assembled nanocomposites (MEβ-NPs) composed of (−)-Epigallocatechin-3-gallate (EGCG), the main catechin in green tea, could sustain release and improve anticancer effects *in vitro* and *in vivo* than free EGCG [23]. The development of nano delivery systems has significantly improved therapeutic efficacy and reduced the side effects of anticancer agents. It was reported that the all-organic nanobullets (denoted as ZPA@HA-ACVA-AZ NBs) developed by combining TDT, PTT, and FCL nanosheets (NSs) obtained from Clay-based nanomaterials had great potential in cancer therapy and diagnostics [24,25]. Epoxy/boron nitride (BN)-poly (vinylidene difluoride) (PVDF) composite exhibited high thermal conductivity with low loading of BN, therefore, it is promising to be used as thermal management materials in advanced electronic devices [26]. Yang and

his colleagues developed a multifunctional nanobullet to effectively treat "immune cold" tumors by reprogramming immunosuppressive tumor microenvironment (TME) toward an immunostimulatory phenotype [27]. Thus, it is essential to find high-efficiency and low-toxicity anti-cancer drugs from natural products and a combination of anti-cancer drugs with nano-carriers for cancer treatment.

Curcuma mainly contains curcumin and volatile oil. Curcumin, a naturally occurring polyphenol, has various biological effects, including antioxidant, antimicrobial, anti-inflammatory, and anticancer potentials [28]. Curcumin induced autophagy and apoptosis by down-regulating Sp1/EGFR activity and inhibiting ERK/MEK and AKT/S6K pathways, thereby enhancing the inhibition of gefitinib on primary gefitinib-resistant NSCLC cell lines H157 and H1299 [29]. In addition, curcumin also exerted anti-lung cancer effects through mechanisms such as inhibition of cell proliferation, invasion and metastasis, epigenetic changes, and regulation of microRNA expression [30]. However, the clinical application of curcumin was limited by its low water solubility,
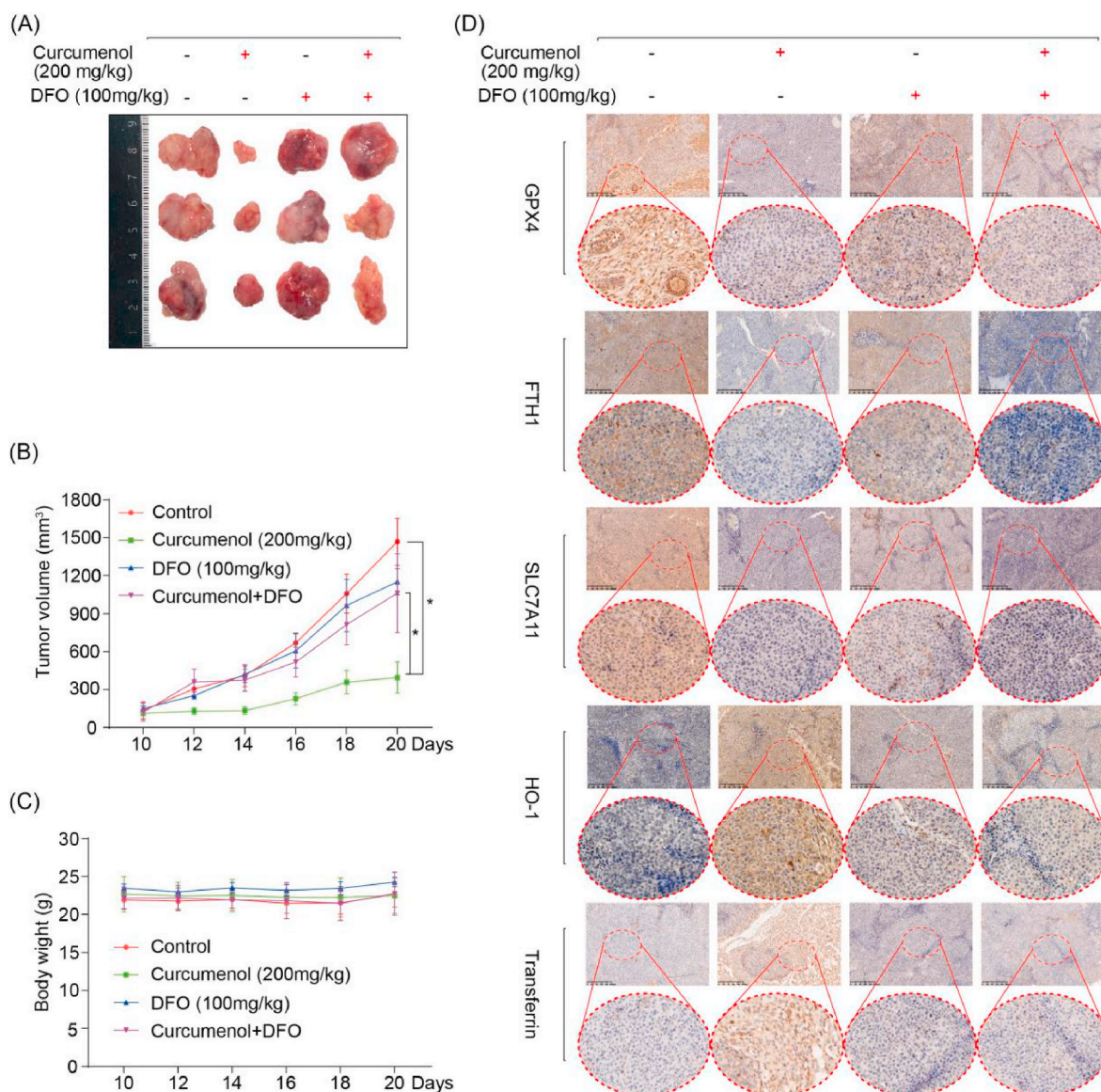
Fig. 5. Curcumenol triggered ferroptosis in the lung cancer xenograft model. (A) A photograph of tumor samples in each group. (B, C) Tumor volumes and mice body weights were measured. (D) The GPX4, FTH1, SLC7A11, HO-1 and transferrin were determined by IHC. *P < 0.05.

poor bioavailability and rapid metabolism [31]. Various nanotechnologies have been tried to change curcumin's physical and chemical properties and its distribution in the body [32–35]. These studies provide new research insights for the development and clinical application of natural compounds.

At present, more than 20 components such as curcumol, isocurcumol, curcumone, and curcumenol have been separated from the volatile oil. Curcumol, curcumone, and curcumenol are high in volatile oil and are considered the main anti-tumor ingredients. Curcumol and curcumenol are both sesquiterpenoids. It has been reported that curcumol exhibited anti-inflammatory and anti-cancer effects in multiple tumor cell lines without significant side effects [36]. Curcumol activated the ROS/CHOP/DR5 signaling pathway by targeting NQO2 to increase the sensitivity of non-small cell lung cancer to TRAIL [37]. Curcumol decreased mouse melanoma B16 cell proliferation and migration by suppressed ERK/NF-κB signaling and c-MET/PI3K/AKT signaling pathway [38]. Isocurcumenol inhibited the proliferation of cancer cells and reduced the ascitic tumor in DLA-challenged mice [39]. Curcumenol could suppress the growth of breast cancer by inhibiting proliferation and inducing apoptosis [40]. Curcumenol also inhibited the growth and

metastasis of liver cancer via reducing endogenous H_2S levels and down-regulating the pSTAT3/BCL-2 and VEGF pathway [7]. Curcumenol exerted antitumor activity and inhibited hepatoma cell HepG2 growth via apoptosis changes [41]. Curcumenol induced the apoptosis of SW1116 cells through down-regulation of Bcl-2 and Bcl-XL and up-regulation of caspase-3 [42]. However, the effect and molecular mechanism of curcumenol in lung cancer are largely unknown. In our research, we investigated the role of curcumenol in lung cancer cells and its underlying molecular mechanisms.

Ferroptosis is an iron-dependent form of non-apoptotic cell death, which has distinct morphologic features and molecular mechanisms. GPX4 is a selenoenzyme that depends on glutathione (GSH). When the activity of GPX4 is inhibited, lipid hydroperoxides significantly accumulate, leading to ferroptosis [43]. SLC7A11, also known as xCT, is a cystine/glutamate antiporter. When the activity of SLC7A11 is inhibited, cystine uptake and glutathione biosynthesis are decreased, thereby inducing ferroptosis [44]. FTH1 is the heavy subunit of ferritin, which plays an essential role in maintaining the balance of iron metabolism in cells. Its level affects the susceptibility to ferroptosis *in vitro* and *in vivo* [45]. ROS accumulation is one of the hallmarks of ferroptosis [19]. The
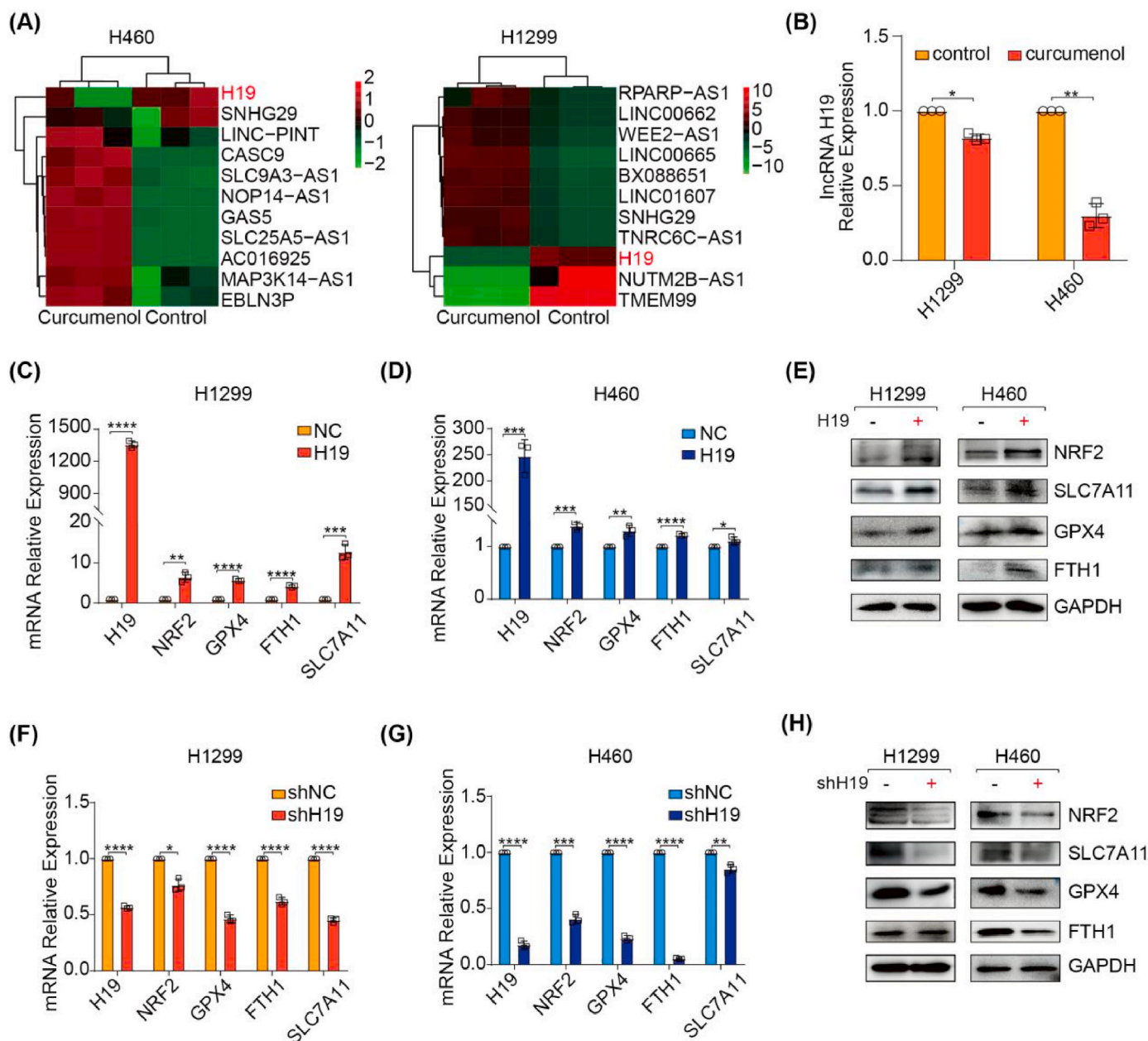
Fig. 6. The correlation between lncRNA H19 expression and curcumenol-induced ferroptosis. (A) Heatmap analysis of the differentially expressed transcripts in lung cancer cells treated with curcumenol. (B) The expression of lncRNA H19 was detected by qRT-PCR after the treatment with curcumenol (300 μg/ml) for 24 h. (C, D) qRT-PCR was used to detect the ferroptosis-related genes in H1299 and H460 cells after lncRNA H19 overexpression. (E) Western blotting was used to detect ferroptosis-related proteins in H1299 and H460 cells after lncRNA H19 overexpression. (F, G) qRT-PCR was used to detect the ferroptosis-related genes in H1299 and H460 cells after lncRNA H19 knockdown. (H) Western blotting was used to detect ferroptosis-related proteins in H1299 and H460 cells after lncRNA H19 knockdown. *P < 0.05, **P < 0.01, ***P < 0.001, ****P < 0.0001, n = 3.

regulation of ROS levels is critical to the determination of cell homeostasis and cell fate. NIR-II fluorescent molecules, ROS sensitive groups and traditional platinum drugs were used to form nanoparticles with NIR-II luminescence capabilities, which can be used for monitoring drugs *in vivo* and therapeutic effect feedback in real-time [46]. Surface-oxidized arsenene nanosheets (As/AsxOy NSs) were found to could catalyze both the reduction of O_2 and oxidation of GSH, inducing ROS aggregation directly and indirectly, respectively [47]. Moreover, PEGylated arsenic nanodots (AsNDs@PEG) were shown to selectively produce large amounts of ROS in tumor cells and combine with β-elemene to achieve synergistic antitumor outcomes [48]. Based on this, the development of nano-Chinese medicine preparations that induce ferroptosis is expected to open a new chapter in lung cancer treatment.

Recently, increasing studies on ferroptosis in cancer have promoted the perspective of using ferroptosis regulators in cancer therapeutics [49]. Several natural products are reported to play an essential role in ferroptosis. Therefore, developing ferroptosis inducer from traditional Chinese medicine might be a promising strategy for cancer treatment. In our research, we demonstrated that curcumenol, isolated from Curcuma wenyujin, exerted its antitumor activities in lung cancer cells through inducing ferroptosis for the first time, as evidenced by ROS generation, GSH depletion, lipid peroxidation, and iron accumulation. In addition, pre-treatment with the ferroptosis inhibitors (Fer-1, Lip-1 and DFO) instead of Nec-1, Z-VAD or CQ eliminated curcumenol-induced cell death both *in vitro* and *in vivo*, suggesting that ferroptosis was the predominant method of curcumenol-triggered cell death.
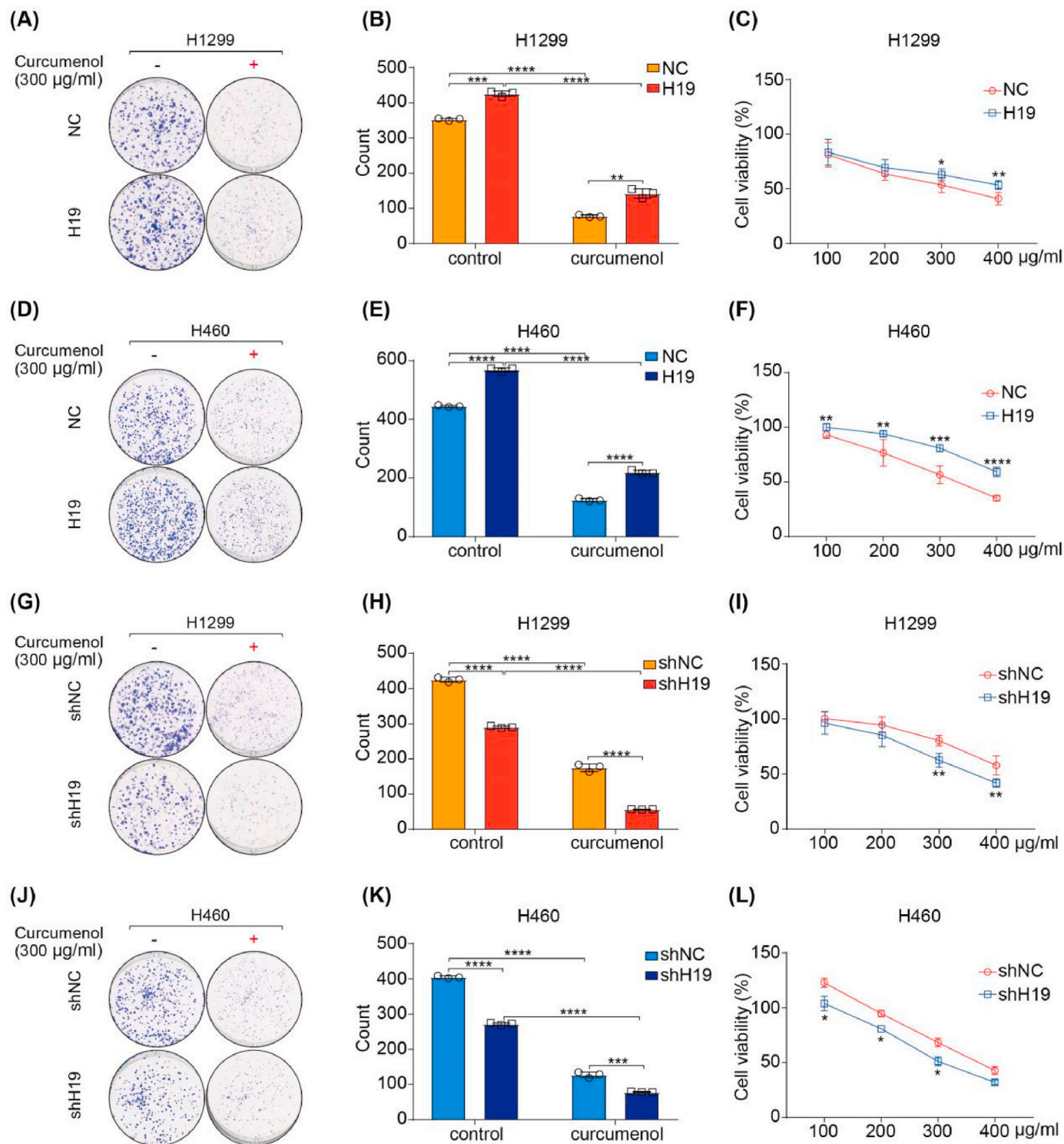
Fig. 7. The effects of lncRNA H19 on curcumenol-induced ferroptosis. (A, B) The colony formation assay was utilized to detect cell proliferation of H1299 cells in response to the treatment with curcumenol (300 μg/ml) alone or in combination with lncRNA H19 overexpression. (C) CCK-8 assays were used to detect the cell viability of H1299 cells in response to the treatment with curcumenol alone or in combination with lncRNA H19 overexpression for 24 h. (D, E) The colony formation assay was utilized to detect cell proliferation of H460 cells in response to the treatment with curcumenol (300 μg/ml) alone or in combination with lncRNA H19 overexpression. (F) CCK-8 assays were used to detect the cell viability of H460 cells in response to the treatment with curcumenol alone or in combination with lncRNA H19 overexpression for 24 h. (G, H) The colony formation assay was utilized to detect cell proliferation of H1299 cells in response to the treatment with curcumenol (300 μg/ml) alone or in combination with lncRNA H19 knockdown. (I) CCK-8 assays were used to detect the cell viability of H1299 cells in response to the treatment with curcumenol alone or in combination with lncRNA H19 knockdown for 24 h. (J, K) The colony formation assay was utilized to detect cell proliferation of H460 cells in response to the treatment with curcumenol (300 μg/ml) alone or in combination with lncRNA H19 knockdown. (L) CCK-8 assays were used to detect the cell viability of H460 cells in response to the treatment with curcumenol alone or in combination with lncRNA H19 knockdown for 24 h *P < 0.05, **P < 0.01, ***P < 0.001, ****P < 0.0001, n = 3.
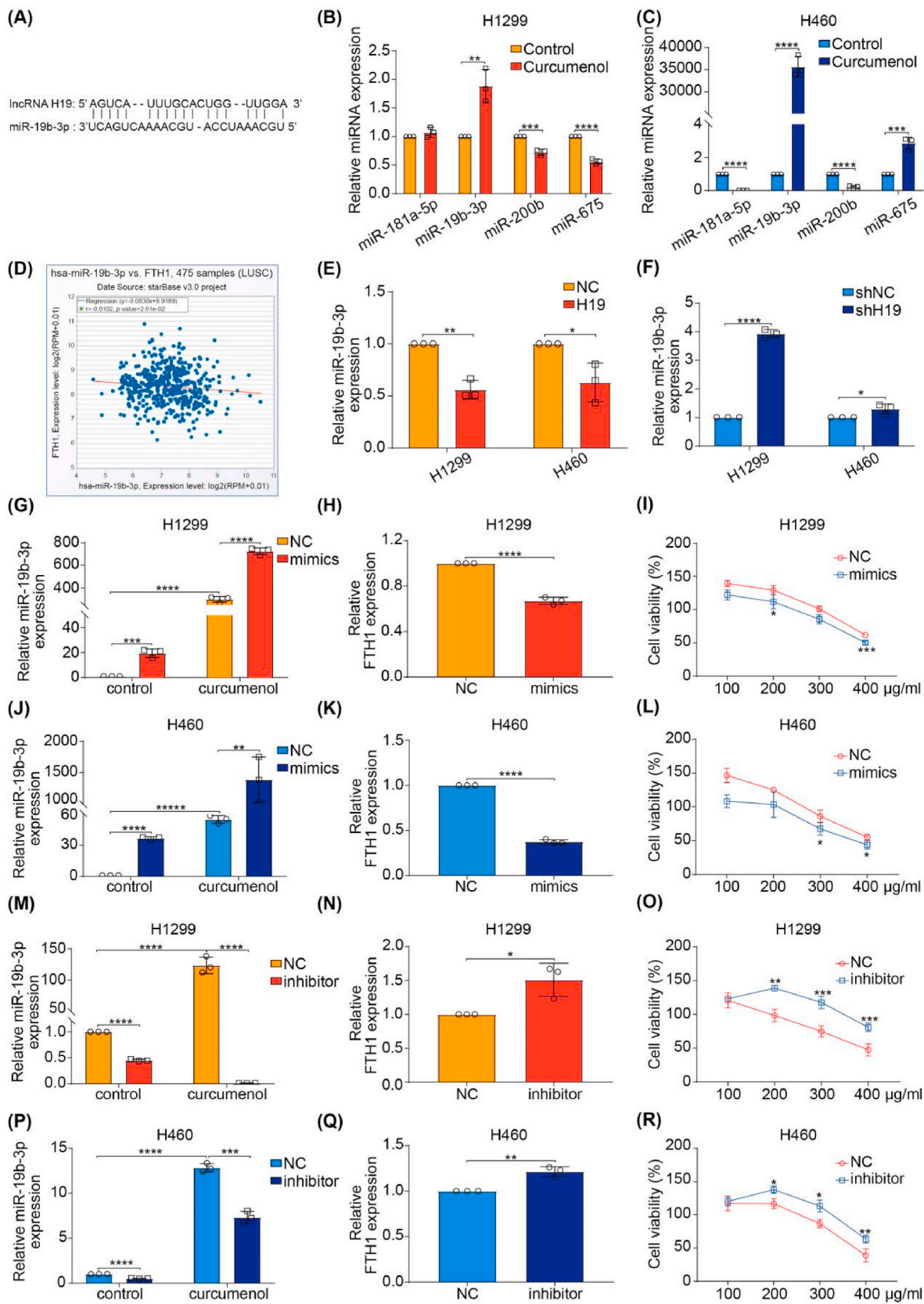
(caption on next page)

Fig. 8. Curcumenol induced ferroptosis in lung cancer cells via lncRNA H19/miR-19b-3p/FTH1 axis. (A) Sequence alignment of miR-19b-3p with the putative binding sites with lncRNA H19. (B, C) qRT-PCR was used to detected miR-181a-5p, miR-19b-3p, miR-200b, miR-675 levels in H1299 and H460 cells after treated with curcumenol (300 μg/ml) for 24 h. (D) Pan-cancer analysis was used to analyze the correlation of miR-19b-3p and FTH1 expression levels in lung squamous cell carcinoma (LUSC). (E, F) The effect of lncRNA H19 on miR-19b-3p was detected by qRT-PCR in H1299 and H460 cells, respectively. (G) qRT-PCR was used to detected miR-19b-3p level in H1299 cells. (H) The FTH1 level in H1299 cells was measured by qRT-PCR. (I) CCK-8 assay was used to analyze the cell viability of H1299 cells in response to the treatment with curcumenol alone or combined with miR-19b-3p mimics. (J) qRT-PCR was used to detected miR-19b-3p level in H460 cells. (K) The FTH1 level in H460 cells was measured by qRT-PCR. (L) CCK-8 assay was used to analyze the cell viability of H460 cells in response to the treatment with curcumenol alone or combined with miR-19b-3p mimics. (M) qRT-PCR was used to detected miR-19b-3p level in H1299 cells. (N) The FTH1 level in H1299 cells was measured by qRT-PCR. (O) CCK-8 assay was used to analyze the cell viability of H1299 cells in response to the treatment with curcumenol alone or combined with miR-19b-3p inhibitor. (P) qRT-PCR was used to detected miR-19b-3p level in H460 cells. (Q) The FTH1 level in H460 cells was measured by qRT-PCR. (R) CCK-8 assay was used to analyze the cell viability of H460 cells in response to the treatment with curcumenol alone or combined miR-19b-3p inhibitor. The $*P < 0.05$, $**P < 0.01$, $***P < 0.001$, $****P < 0.0001$, n = 3.

To determine the molecular mechanism of ferroptosis induced by curcumenol, RNA sequencing was performed. As a result, lncRNA H19 was significantly downregulated in H1299 and H460 cells treated with curcumenol. In further research, we found that lncRNA H19 over-expression significantly abolished the anticancer effect of curcumenol in H1299 and H460 cells and subsequently increased the expression of ferroptosis negative regulatory factors (NRF2, GPX4, FTH1, and SLC7A11). Therefore, lncRNA H19 might be a potential target of curcumenol-induced ferroptosis in lung cancer cells.

It was reported that lncRNAs exerted their biological functions by acting as a ceRNA or interacting with RNA-binding proteins [16–18]. In our research, we found that lncRNA H19 inhibited the expression level of FTH1 through sponging miR-19b-3p. The miR-19b-3p mimics deceased the FTH1 expression but increased the anticancer activity of curcumenol. On the contrary, miR-19b-3p inhibitor increased FTH1 expression but abrogated the anticancer activity of curcumenol. Based on that, our data demonstrated that lncRNA H19 regulated FTH1 expression by targeting miR-19b-3p, which.

In conclusion, our data demonstrated that the natural product curcumenol exhibited its antitumor activity by triggering ferroptosis both *in vitro* and *in vivo* for the first time. Mechanistically, the lncRNA H19/miR-19b-3p/FTH1 axis was essential for curcumenol-induced ferroptotic cell death. Our study will provide potential therapeutic agents for lung cancer patients.

Declaration of competing interest

All authors declare that they have no conflict of interest.

Credit author statement

Ruonan Zhang: Designed the experiments, carried out all the experiments, analyzed the original data, and wrote the original draft. **Ting Pan:** Wrote the paper and analyzed the partial data. **Yu Xiang:** Formal analysis, data curation, and wrote the paper. **Mingming Zhang:** Analyzed the partial data. **Han Xie:** Analyzed the partial data. **Zimao Liang:** Analyzed the partial data. **Bi Chen:** Designed the animal experiments and analyzed the data. **Cong Xu:** Carried out partial experiments. **Jing Wang:** Analyzed the partial data. **Xingxing Huang:** Analyzed the partial data. **Qianru Zhu:** Analyzed the partial data. **Ziming Zhao:** Carried out the partial experiments. **Quan Gao:** Carried out the partial experiments. **Chengyong Wen:** Analyzed the partial data. **Wencheng Liu:** Analyzed the partial data. **Weirui Ma:** Analyzed the partial data. **Jiao Feng:** Contributed to design the experiments. **Xueni Sun:** Designed the experiments. **Ting Duan:** Designed the experiments. **Elaine Lai-Han Leung:** Designed the experiments. **Tian Xie:** Project administration. **Qibiao Wu:** Writing - review & editing, Supervision. **Xinbing Sui:** Conceptualization, Review & editing the text, Project administration.

Acknowledgment

Appendix A. Supplementary data

Supplementary data to this article can be found online at https://doi.org/10.1016/j.bioactmat.2021.11.013.

References

[1] Sung, J. Ferlay, R. Siegel, M. Laversanne, I. Soerjomataram, A. Jemal, F. Bray, Global cancer statistics 2020: GLOBOCAN estimates of incidence and mortality worldwide for 36 cancers in 185 countries, CA A Cancer J. Clin. 71 (2021) 209–249.

[2] J. Wang, K. Zou, X. Feng, M. Chen, C. Li, R. Tang, Y. Xuan, M. Luo, W. Chen, H. Qiu, G. Qin, Y. Li, C. Zhang, B. Xiao, L. Kang, T. Kang, W. Huang, X. Yu, X. Wu, W. Deng, Downregulation of NMI promotes tumor growth and predicts poor prognosis in human lung adenocarcinomas, Mol. Cancer 16 (2017) 158.

[3] M. Kim, C. Cervantes, Y. Jung, X. Zhang, J. Zhang, S.H. Lee, S. Jun, L. Litovchick, W. Wang, J. Chen, B. Fang, J. Park, PAF remodels the DREAM complex to bypass cell quiescence and promote lung tumorigenesis, Mol. Cell 81 (2021) 1698–1714.

[4] Z. Li, Z. Feiyue, L. Gaofeng, Traditional Chinese medicine and lung cancer–from theory to practice, Biomed. Pharmacother. 137 (2021) 111381.

[5] E. Jung, T. Trinh, T. Lee, N. Yamabe, K. Kang, J. Song, S. Choi, S. Lee, T. Jang, K. Kim, G. Hwang, Curcuzedoalide contributes to the cytotoxicity of Curcuma zedoaria rhizomes against human gastric cancer AGS cells through induction of apoptosis, J. Ethnopharmacol. 213 (2018) 48–55.

[6] T. Lee, D. Lee, S. Lee, Y. Ko, K. Sung Kang, S. Chung, K. Kim, Sesquiterpenes from Curcuma zedoaria rhizomes and their cytotoxicity against human gastric cancer AGS cells, Bioorg. Chem. 87 (2019) 117–122.

[7] H. Han, L. Wang, Y. Liu, X. Shi, X. Zhang, M. Li, T. Wang, Combination of Curcuma zedoary and kelp inhibits growth and metastasis of liver cancer in vivo and in vitro via reducing endogenous HS levels, Food Funct. 10 (2019) 224–234.

[8] X. Han, Y. Ye, B. Guo, S. Liu, Effects of platycodin D in combination with different active ingredients of Chinese herbs on proliferation and invasion of 4T1 and MDA-MB-231 breast cancer cell lines, Zhong Xi Yi Jie He Xue Bao 10 (2012) 67–75.

[9] M. Ai-Amin, N. Eltayeb, M. Khairuddean, S. Salhimi, Bioactive chemical constituents from Curcuma caesia Roxb. rhizomes and inhibitory effect of Curcuzederone on the migration of triple-negative breast cancer cell line MDA-MB-231, Nat. Prod. Res. 15 (2019) 1–5.

[10] H. Yan, T. Zou, Q. Tuo, S. Xu, H. Li, A. Belaidi, P. Lei, Ferroptosis: mechanisms and links with diseases, Signal Transduct. Target. Ther. 6 (2021) 49.

[11] B. Hassannia, P. Vandenabeele, T. Vanden Berghe, Targeting ferroptosis to iron out cancer, Cancer Cell 35 (2019) 830–849.

[12] J. Ye, R. Zhang, F. Wu, L. Zhai, K. Wang, M. Xiao, T. Xie, X. Sui, Non-apoptotic cell death in malignant tumor cells and natural compounds, Cancer Lett. 420 (2018) 210–227.

[13] J. Wang, S. Xie, J. Yang, H. Xiong, Y. Jia, Y. Zhou, Y. Chen, X. Ying, C. Chen, C. Ye, L. Wang, J. Zhou, The long noncoding RNA H19 promotes tamoxifen resistance in breast cancer via autophagy, J. Hematol. Oncol. 12 (2019) 81.

[14] P. Wang, S. Ning, Y. Zang, R. Li, J. Ye, Z. Zhao, H. Zhi, T. Wang, Z. Guo, Xia Li, Identification of lncRNA-associated competing triplets reveals global patterns and prognostic markers for cancer, Nucleic Acids Res. 43 (2015) 3478–3489.

[15] Y. Tay, J. Rinn, P. Pandolfi, The multilayered complexity of ceRNA crosstalk and competition, Nature 505 (2014) 344–352.

[16] J. Yang, Q. Qiu, X. Qian, J. Yi, Y. Jiao, M. Yu, X. Li, J. Li, C. Mi, J. Zhang, B. Lu, E. Chen, P. Liu, Y. Lu, Long noncoding RNA LCAT1 functions as a ceRNA to regulate RAC1 function by sponging miR-4715-5p in lung cancer, Mol. Cancer 18 (2019) 171.

[17] C. Zhou, C. Yi, Y. Y, W. Qin, Y. Yan, X. Dong, X. Zhang, Y. Huang, R. Zhang, J. Wei, D. Ali, M. Michalak, X. Chen, J. Tang, LncRNA PVT1 promotes gemcitabine resistance of pancreatic cancer via activating Wnt/β-catenin and autophagy pathway through modulating the miR-619-5p/Pygo2 and miR-619-5p/ATG14 axes, Mol. Cancer 19 (2020) 118.

[18] Y. Gao, F. Wu, J. Zhou, L. Yan, M. Jurczak, H. Lee, L. Yang, M. Mueller, X. Zhou, L. Dandolo, J. Szendroedi, M. Roden, C. Flannery, H. Taylor, G. Carmichae, G. Shulman, Y. Huang, The H19/let-7 double-negative feedback loop contributes to glucose metabolism in muscle cells, Nucleic Acids Res. 42 (2014) 13799–13811.

[19] Z. Zhang, M. Guo, Y. Li, M. Shen, D. Kong, J. Shao, H. Ding, S. Tan, A. Chen, F. Zhang, S. Zheng, RNA-binding protein ZFP36/TTP protects against ferroptosis by regulating autophagy signaling pathway in hepatic stellate cells, Autophagy 16 (2020) 1482–1505.

[20] J.J. Chan, Z.H. Kwok, X.H. Chew, B. Zhang, C. Liu, T.W. Soong, H. Yang, Y. Tay, A FTH1 gene:pseudogene: microRNA network regulates tumorigenesis in prostate cancer, Nucleic Acids Res. 46 (2018) 1998–2011.

[21] G. Blumenthal, S. Karuri, H. Zhang, L. Zhang, S. Khozin, D. Kazandjian, S. Tang, R. Sridhara, P. Keegan, R. Pazdur, Overall response rate, progression-free survival, and overall survival with targeted and standard therapies in advanced non-small-cell lung cancer: US Food and Drug Administration trial-level and patient-level analyses, J. Clin. Oncol. 33 (2015) 1008–1014.

[22] D. Vergara, C. Bellomo, X. Zhang, V. Vergaro, A. Tinelli, V. Lorusso, R. Rinaldi, Y. Lvov, S. Leporatti, M. Maffia, Lapatinib/Paclitaxel polyelectrolyte nanocapsules for overcoming multidrug resistance in ovarian cancer, Nanomedicine 8 (2012) 891–899.

[23] Y. Yang, P. Jin, X. Zhang, N. Ravichandran, H. Ying, C. Yu, H. Ying, Y. Xu, J. Yin, K. Wang, M. Wu, Q. Du, New Epigallocatechin Gallate (EGCG) Nanocomplexes co-assembled with 3-mercapto-1-hexanol and β-lactoglobulin for improvement of antitumor activity source, J. Biomed. Nanotechnol. 13 (2017) 805–814.

[24] D. Gao, T. Chen, S. Chen, X. Ren, Y. Han, Y. Li, Y. Wang, X. Guo, H. Wang, X. Chen, M. Guo, Y. Zhang, G. Hong, X. Zhang, Z. Tian, Z. Yang, Targeting hypoxic tumors with hybrid nanobullets for oxygen-independent synergistic photothermal and thermodynamic therapy, Nano-Micro Lett. 13 (2021) 99.

[25] X. Ji, L. Ge, C. Liu, Z. Tang, Y. Xiao, W. Chen, Z. Lei, W. Gao, S. Blake, D. De, B. Shi, X. Zeng, N. Kong, X. Zhang, W. Tao, Capturing functional two-dimensional nanosheets from sandwich-structure vermiculite for cancer theranostics, Nat. Commun. 12 (2021) 1124.

[26] X. Chen, J. Lim, W. Yan, F. Guo, Y. Liang, H. Chen, A. Lambourne, X. Hu, Salt template assisted bn scaffold fabrication toward highly thermally conductive epoxy composites, ACS Appl. Mater. Interfaces 12 (2020) 16987–16996.

[27] Z. Yang, D. Gao, X. Guo, L. Jin, J. Zheng, Y. Wang, S. Chen, X. Zheng, L. Zeng, M. Guo, X. Zhang, Z. Tian, Fighting immune cold and reprogramming immunosuppressive tumor microenvironment with red blood cell membrane-camouflaged nanobullets, ACS Nano 14 (2020) 17442–17457.

[28] K. Sanidad, E. Sukamtoh, H. Xiao, D. McClements, G. Zhang, Curcumin: recent advances in the development of strategies to improve oral bioavailability, Annu. Rev. Food Sci. Technol. 10 (2019) 597–617.

[29] P. Chen, H. Huang, Y. Wang, J. Jin, W. Long, K. Chen, X. Zhao, C. Chen, J. Li, Curcumin overcome primary gefitinib resistance in non-small-cell lung cancer cells through inducing autophagy-related cell death, J. Exp. Clin. Cancer Res. 38 (2019) 254.

[30] W. Wan, N. Lajis, F. Abas, I. Othman, R. Naidu, Mechanistic understanding of Curcumin's therapeutic effects in lung cancer, Nutrients 11 (2019) 2989.

[31] Y. He, H. Liu, W. Bian, Y. Liu, X. Liu, S. Ma, X. Zheng, Z. Du, K. Zhang, D. Ouyang, Molecular interactions for the Curcumin-polymer complex with enhanced anti-inflammatory effects, Pharmaceutics 11 (2019) 442.

[32] Y. Wang, D. Gao, Y. Liu, X. Guo, S. Chen, L. Zeng, J. Ma, X. Zhang, Z. Tian, Z. Yang, Immunogenic-cell-killing and immunosuppression-inhibiting nanomedicine, Bioact. Mater. 6 (2020) 1513–1527.

[33] Z. Zheng, X. Zhang, D. Carbo, C. Clark, C. Nathan, Y. Lvov, Sonication-assisted synthesis of polyelectrolyte-coated Curcumin nanoparticles, Langmuir 26 (2010) 7679–7681.

[34] X. Chen, Y. Chen, L. Zou, X. Zhang, Y. Dong, J. Tang, D. McClements, W. Liu, Plant-based nanoparticles prepared from proteins and phospholipids consisting of a core-multilayer-shell structure: fabrication, stability, and foamability, J. Agric. Food Chem. 67 (2019) 6574–6584.

[35] D. Gao, X. Guo, X. Zhang, S. Chen, Y. Wang, T. Chen, G. Huang, Y. Gao, Z. Tian, Z. Yang, Multifunctional phototheranostic nanomedicine for cancer imaging and treatment, Mater. Today Bio. 5 (2019) 100035.

[36] Y. Jia, F. Wang, Q. Guo, M. Li, L. Wang, Z. Zhang, S. Jiang, H. Jin, A. Chen, S. Tan, F. Zhang, J. Shao, S. Zheng, Curcumol induces RIPK1/RIPK3 complex- dependent necroptosis via JNK1/2-ROS signaling in hepatic stellate cells, Redox Biol 19 (2018) 375–387.

[37] J. Zhang, Y. Zhou, N. Li, W. Liu, J. Liang, Y. Sun, W. Zhang, R. Fang, S. Huang, Z. Sun, Y. Wang, Q. He, Curcumol overcomes TRAIL resistance of non-small cell lung cancer by targeting NRH:Quinone Oxidoreductase 2 (NQO2), Adv. Sci. (Weinh.) 7 (2020) 2002306.

[38] N. Ning, S. Liu, X. Liu, Z. Tian, Y. Jiang, N. Yu, B. Tan, H. Feng, X. Feng, L. Zou, Curcumol inhibits the proliferation and metastasis of melanoma via the miR-152-3p/PI3K/AKT and ERK/NF-κB signaling pathways, J. Cancer 11 (2020) 1679–1692.

[39] S. Lakshmi, G. Padmaja, P. Remani, Antitumour effects of Isocurcumenol isolated from Curcuma zedoaria Rhizomes on human and murine cancer cells, Int. J. Med. Chem. 2011 (2011) 253962.

[40] F. Nur, R. Muhaimin, Widodo, Curcuma zedoaria: potential effect as breast cancer chemotherapeutic agents through CXCR4 inhibition, AIP Conf. Proc. 2231 (2020), 040028.

[41] E. Abdel-Lateef, F. Mahmoud, O. Hammam, E. El-Ahwany, E. El-Wakil, S. Kandil, H. Abu, M. El-Sayed, H. Hassenein, Bioactive chemical constituents of Curcuma longa L. rhizomes extract inhibit the growth of human hepatoma cell line (HepG2), Acta Pharm. 66 (2016) 387–398.

[42] X. Du, P. Feng, Y. Hou, H. Qin, Y. Han, Y. Zhang, Effects of proliferation inhibition and apoptosis induction of Curcumol on SW1116 cells and its mechanism, Sci. Technol. Eng. 28 (2010).

[43] W. Yang, R. SriRamaratnam, M. Welsch, K. Shimada, R. Skouta, V. Viswanathan, J. Cheah, P. Clemons, A. Shamji, C. Clish, L. Brown, A. Girotti, V. Cornish, S. Schreiber, B. Stockwell, Regulation of ferroptotic cancer cell death by GPX4, Cell 156 (2014) 317–331.

[44] P. Koppula, Y. Zhang, L. Zhuang, B. Gan, Amino acid transporter SLC7A11/xCT at the crossroads of regulating redox homeostasis and nutrient dependency of cancer, Cancer Commun. 38 (2018) 12.

[45] Y. Fang, X. Chen, Q. Tan, H. Zhou, J. Xu, Q. Gu, Inhibiting ferroptosis through disrupting the NCOA4-FTH1 interaction: a new mechanism of action, ACS Cent. Sci. 7 (2021) 980–989.

[46] D. Wei, Y. Yu, Y. Huang, Y. Jiang, Y. Zhao, Z. Nie, F. Wang, W. Ma, Z. Yu, Y. Huang, X. Zhang, Z. Liu, X. Zhang, H. Xiao, A Near-Infrared-II Polymer with tandem fluorophores demonstrates superior biodegradability for simultaneous drug tracking and treatment efficacy feedback, ACS Nano 15 (2021) 5428–5438.

[47] N. Kong, H. Zhang, C. Feng, C. Liu, Y. Xiao, X. Zhang, L. Mei, J. Kim, W. Tao, X. Ji, Arsenene-mediated multiple independently targeted reactive oxygen species burst for cancer therapy, Nat. Commun. 12 (2021) 4777.

[48] C. Liu, S. Sun, Q. Feng, G. Wu, Y. Wu, N. Kong, Z. Yu, J. Yao, X. Zhang, W. Chen, Z. Tang, Y. Xiao, X. Huang, A. Lv, C. Yao, H. Cheng, A. Wu, T. Xie, W. Tao, Arsenene nanodots with selective killing effects and their low-dose combination with ß-elemene for cancer therapy, Adv. Mater. 33 (2021), e2102054.

[49] E. Dai, L. Han, J. Liu, Y. Xie, H. Zeh, R. Kang, L. Bai, D. Tang, Ferroptotic damage promotes pancreatic tumorigenesis through a TMEM173/STING-dependent DNA sensor pathway, Nat. Commun. 11 (2020) 6339.